# Spatial structure of hydrography and flow in a Chilean fjord, Estuario Reloncav??

**Article** *in* Estuaries and Coasts · February 2007

DOI: 10.1007/BF02782972

CITATIONS
74

READS
304

**5 authors**, including:

Arnoldo Valle-Levinson
University of Florida
**269** PUBLICATIONS **4,872** CITATIONS
SEE PROFILE

Rosario Sanay
Universidad Veracruzana
**13** PUBLICATIONS **289** CITATIONS
SEE PROFILE

D. Soto
Food and Agriculture Organization of the United Nations
**74** PUBLICATIONS **9,299** CITATIONS
SEE PROFILE

Jorge León-Muñoz
Universidad Católica de la Santísima Concepción (UCSC)
**20** PUBLICATIONS **587** CITATIONS
SEE PROFILE

Estuaries and Coasts Vol. 30, No. 1, p. 113–126 February 2007

# Spatial Structure of Hydrography and Flow in a Chilean Fjord, Estuario Reloncaví

ARNOLDO VALLE-LEVINSON[1,*], NANDITA SARKAR[2], ROSARIO SANAY[3], DORIS SOTO[4,†], and JORGE LEÓN[4]

[1] *Civil and Coastal Engineering, University of Florida, 365 Weil Hall, Gainesville, Florida 32611*
[2] *Center for Coastal Physical Oceanography, Old Dominion University, Norfolk, Virginia 23529*
[3] *Marine Science Program, Department of Geological Sciences, University of South Carolina, Columbia, South Carolina 29208*
[4] *Facultad de Pesquerías y Oceanografía, Universidad Austral de Chile, Puerto Montt, Chile*

**ABSTRACT: Underway current velocity profiles were combined with temperature and salinity profiles at fixed stations to describe tidal and subtidal flow patterns in the middle of the northernmost Chilean fjord, Estuario Reloncaví. This is the first study involving current velocity measurements in this fjord. Reloncaví fjord is 55 km long, 2 km wide, and on average is 170 m deep. Measurements concentrated around a marked bend of the coastline, where an 8-km along-fjord transect was sampled during a semidiurnal tidal cycle in March 2002 and a 2-km cross-fjord transect was occupied, also during a semidiurnal cycle, in May 2004. The fjord hydrography showed a relatively thin (< 5 m deep), continuously stratified, buoyant layer with stratification values > 4 kg m$^{-3}$ per meter of depth. Below this thin layer, the water was relatively homogeneous. Semidiurnal tidal currents had low amplitudes (< 10 cm s$^{-1}$) that allowed the persistence of a surface front throughout the tidal cycle. The front oscillated with a period of ca. 2.5 h and showed excursions of 2 km. The front oscillations could have been produced by a lateral seiche that corresponds to the natural period of oscillation across the fjord. This front could have also caused large (2 h) phase lags in the semidiurnal tidal currents, from one end of the transect to the other, within the buoyant layer. Tidal phases were relatively uniform underneath this buoyant layer. Subtidal flows showed a 3-layer pattern consisting of a surface layer (8 m thick, of 5 cm s$^{-1}$ surface outflow), an intermediate layer (70 m thick, of 3 cm s$^{-1}$ net inflow), and a bottom layer (below 80 m depth, of 3 cm s$^{-1}$ net outflow). The surface outflow and, to a certain extent, the inflow layer were related to the buoyant water interacting with the ambient oceanic water. The inflowing layer and the bottom outflow were attributed to nonlinear effects associated with a tidal wave that reflects at the fjord's head. The weak subtidal currents followed the morphology of the bend and caused downwelling on the inside and upwelling on the outside part of the bend.**

## Introduction

Many fjords in the world are being used for aquaculture activities that affect the water quality of the system and in turn are affected by the hydrodynamics of the fjord. In some fjords of the Chilean Inland Sea (Fig. 1), salmon farming may be affected by hypoxic conditions that develop in near-surface waters (León 2005). The reason for the development of these hypoxic conditions near the surface is not yet completely understood. The northernmost fjord in Chile, Estuario Reloncaví, supports one of Chile's largest salmon farming activities. These activities could affect the ecosystem through nutrient loading (Soto and Norambuena 2004) and, in turn, could be affected by natural physical processes. This study was designed with the purpose of providing a basic understanding on the hydrographic and current velocity characteristics in Estuario Reloncaví. Such basic understanding remains elusive in most systems of the Chilean Inland Sea and shall eventually lead to an understanding of the causes for near-surface hypoxic conditions in these systems.

The hypothesis was that low-oxygen waters below the pycnocline could get close to the surface through an internal lateral seiche, in an analogous way in which nutrients can be pumped to the surface in an estuary (e.g., Malone et al. 1986). The seiche could produce a sequence of upwelling-downwelling pulses at both sides of the fjord. The development of the upwelling-downwelling sequence would probably be related to the flow around a bend or point. This has been described for unidirectional river flow in meandering channels (Bathurst et al. 1977; Thorne and Hey 1979) and in tidal, bidirectional oceanic flows (Geyer and Signell 1990; Signell and Geyer 1991; Geyer 1993; Chant and Wilson 1997; Seim and Gregg 1997).

* Corresponding author; tele: 353/392-9537x1479; fax: 352/392-3394; e-mail: arnoldo@ufl.edu

† Current address: Fisheries and Aquaculture Department, Food and Agriculture Organization of the United Nations, Viale delle Terme di Caracalla 00153, Rome, Italy

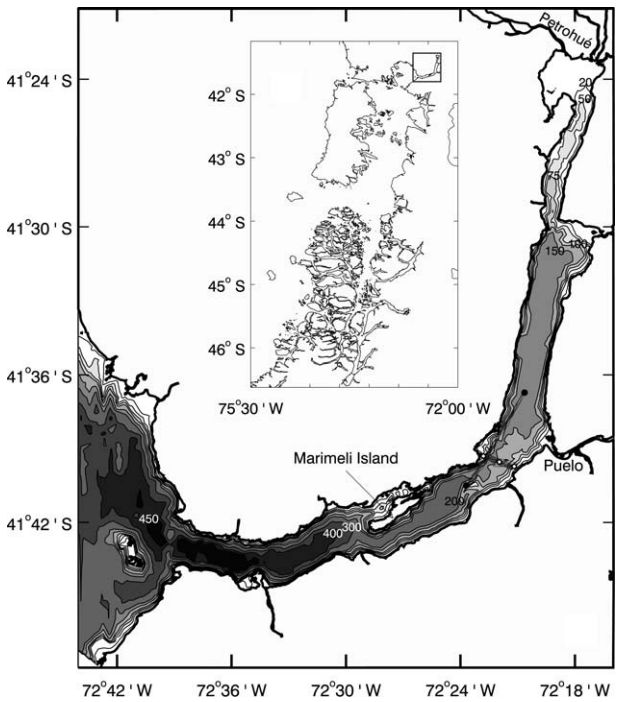


Fig. 1. Estuario Reloncaví in the context of the Chilean Inland Sea. The position of Reloncaví is denoted by a rectangle in the inset map. The fine scale representation shows the 20, 50, 75, 100, 150, 200, 300, 400, 450 and 500 m isobaths. It also displays the CTD stations for along-fjord and across-fjord transects as filled and open circles. Bathymetry provided by M. Cáceres of the Chilean Naval Hydrographic Service.

Although the original sampling plan envisioned exploration of downwelling-upwelling sequences arising from curvature effects, bad weather hindered its execution. The data obtained in this study suggested the presence of a lateral seiche with a period of 2.5 h and illustrated revealing patterns of subtidal exchange flow.

## Study Area

Estuario Reloncaví is the South American fjord closest to the Equator and, being centered at 41.6°S, is one of the most equatorward fjords in the world (Fig. 1). The fjord is 55 km long and less than 3 km at its widest part. The general shape of the fjord emulates an obtuse J as the orientation changes from ca. 10°T in the northern (upper) 27 km to 70°T in the southern (lower) 27 km. Near its head, Reloncaví fjord receives the discharge of the Petrohué River at a mean annual rate of 280 $m^3 s^{-1}$ (León 2005). In the middle portion where it changes orientation, the fjord receives the discharge of the third largest river in Chile, the Puelo, at a mean annual rate of 650 $m^3 s^{-1}$ (Milliman et al. 1995). The river discharge shows strong seasonality, with maxima approaching 900 $m^3 s^{-1}$ in June and minima of 300 $m^3 s^{-1}$ observed in March (León 2005). This river discharge pattern is linked to the precipitation regime in the area and to late spring-early summer ice melts. Precipitation is most intense in late autumn and early winter and exceeds 2 m $yr^{-1}$ at a coastal station in the middle of the fjord (Dirección Meteorológica de Chile: www.meteochile.cl). Given the 700-$km^2$ surface area of the fjord (León 2005) and the 2 m $yr^{-1}$ precipitation, the direct freshwater input to the fjord averages $3.4 \times 10^8$ $m^3 yr^{-1}$ or 11 $m^3 s^{-1}$. This seems to represent only a small fraction of the total freshwater input to the system, but requires further studies because of the very large spatial variability of precipitation patterns in the area. In general, it can be said that Reloncaví fjord receives an annual mean discharge of 900 $m^3 s^{-1}$ (Niemeyer and Cereceda 1984).

The bathymetry of Reloncaví fjord shows a basin $> 400$ m deep between the mouth and Marimeli Island (Fig. 1). This basin is separated from the Inland Sea by a sill of 150 m height that rises to a depth of 300 m (from 450 m). Upstream of Marimeli Island, i.e., toward the fjord's head, the bathymetry exhibits rapid variations associated with the bend where the fjord changes orientation. Further upstream of the bend, the bathymetry changes little throughout a basin $< 200$ m deep. In the upper 10 km of the fjord, the bottom shoals to depths $< 100$ m and the coastline exhibits a marked constriction. The average depth from the mouth to the head is 170 m. Most cross sections of the bathymetry across the fjord show broad areas of maximum depth except around the bend, where the deepest part becomes narrow. The bathymetry is quite steep near the coastlines in most of the fjord except in the bend area, where bottom changes are less abrupt near the coast. This could be related to suspended sediment carried by the Puelo River to the fjord where it deposits in an asymmetric distribution apparently favored by the earth's rotation as sediment is deposited to the south of the river mouth.

The tidal regime in the fjord area is mainly semidiurnal (Fig. 2). The amplitudes of the $M_2$, $S_2$, and $N_2$ constituents inside the fjord are 1.80, 1.09, and 0.40 m, respectively, whereas the amplitudes of the $K_1$ and $O_1$ constituents are 0.19 and 0.17 m, respectively. The form factor, which is the ratio of the sum of diurnal constituents ($K_1 + O_1$) to the sum of semidiurnal constituents ($M_2 + S_2$) yields a value of 0.12, which indicates a semidiurnal regime for tides. The tidal range outside the fjord reaches values close to 12 m (Cáceres et al. 2003). Inside the fjord, the tidal range is between 6 and 7 m during spring tides and decreases to 1 m in neap tides. Tidal currents are typically $< 0.1$ m $s^{-1}$ and the tidal wave in the fjord is nearly stationary as

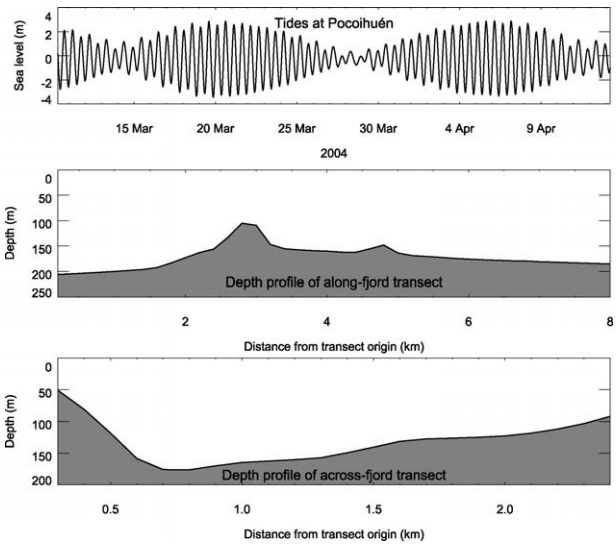


Fig. 2. Tides measured at Pocoihuén, near the head of the fjord, and bathymetry of along-fjord (looking toward the west; the southern end of the transect is to the left) and across-fjord (looking into the fjord; west is to the left) transects.

tidal currents and sea levels are close to 90° out of phase.

Wind forcing in the area exhibits well defined seasonality. Northerly winds dominate in the spring and summer and tend to be weaker than winter winds that blow predominantly from the south. Sporadic spring-summer northerly winds can exceed 10–15 m $s^{-1}$ (Cáceres et al. 2002; Valle-Levinson and Blanco 2004). Given the strong winds that typically affect the region and the restricted choice in vessels available in the area, it is challenging to obtain data sets like the one presented in this study. The data set represents the first one of its kind in Reloncaví fjord.

## Data Collection and Processing

Current velocity and density profiles were obtained during semidiurnal periods at transects that spanned the region of the fjord where the coastline orientation changes (Fig. 1). The area of orientation change was the focus of the sampling effort because of three main reasons: this is the area of the fjord where the hypothesis of lateral oscillations of the pycnocline favoring near-surface hypoxia could be explored; this is also the area where several salmon aquaculture facilities are placed; and except for the shallow portion at the fjord's head, this is the region where the bottom is shallow enough for it to be tracked by the current profiler. It turns out that because the currents are so weak (0.1 m $s^{-1}$), it is essential to be able to track the bottom with the instrument in order to assure the quality of the data. An along-fjord transect was sampled on March 10, 2002, between neap and spring tides, and an across-fjord transect was occupied on May 5, 2004, during spring tides. The original plan was to sample along-fjord and across-fjord transects consecutively but weather conditions hindered data collection for several days after the along-fjord sampling in March 2002. A return trip to the study area in May 2004 allowed sampling across the fjord.

The along-fjord transect (Fig. 1) extended for 8 km at an orientation of 30°T and was limited by two hydrographic stations located at 41.675°S, 72.394°W and 41.612°S, 72.345°W. The transect was occupied 9 times with the barge *Triton* during 10 h on March 10, 2002. Each transect repetition took over 1 h to complete, so the data were not synoptic. The across-fjord transect extended for 2 km at an orientation of 110°T and was also constrained by two hydrographic stations located at 41.654°S, 72.381°W and 41.662°S, 72.354°W. An additional hydrographic station was occupied in the middle of the transect at 41.660°S, 72.367°W. This transect was repeated 21 times onboard the M/B *San Pedro* during 12 h on May 5, 2004.

In both sampling periods, water velocity profiles were obtained underway with a 307.2 kHz RD Instruments Acoustic Doppler Current Profiler (ADCP) mounted on a catamaran and towed off the starboard side of the vessel at speeds between 2 and 2.5 m $s^{-1}$. Each ADCP ping was recorded at 2-m bins, every 2 s. The average of 15 pings yielded a temporal resolution of 30 s or a spatial resolution of 60 to 75 m. The first usable bin was located at a depth of 3.4 m and the last usable bin reached depths around 100 m. Navigation data were collected with a Garmin GPSMAP 185 global positioning system (GPS). The same velocity data collection procedures were used for both along-fjord and across-fjord transects.

Profiles of temperature and salinity were recorded at 2 Hz at the two ends of the along-fjord transect with a SeaBird SBE-19 conductivity-temperature-depth (CTD) profiler. The CTD profiles reached depths between 80 and 100 m, instead of the local depth of the station (200 m) as properties changed negligibly below 20 m. A total of 5 CTD casts per station were recorded in the along-fjord transect on March 10, 2002. Data were processed with the manufacturer's software in order to align sensors, eliminate loops, and average to 1-m bins. In addition to the CTD stations, a SeaBird SBE-37 conductivity-temperature (CT) sensor was attached to the catamaran to measure underway surface temperature and salinity every 30 s. In the May 2004 across-fjord transect, an Idromar's IM51 Multiparameter probe was used to collect profiles of temperature, conductivity, and dissolved oxygen (DO) at 0.2 Hz at both ends and in the middle of

the transect. The accuracy of the Idromar probe instruments is 0.02°C, 0.02 mS $cm^{-1}$, and 2% saturation, for temperature, conductivity, and DO, respectively. These are adequate accuracies for the large gradients observed in the surface layer of the system. The Idromar's profiles were recorded to depths of 30 m at the ends of the transect and 60 m in the middle. Below depths of 10 m, properties changed insignificantly.

The ADCP data were trimmed using the criteria described by Valle-Levinson and Atkinson (1999). The current directions, as determined with the ADCP compass, were calibrated with GPS data following the method described by Joyce (1989). This procedure was followed by arranging every transect repetition onto a regular distance versus depth grid. The vertical grid size was 2 m and the horizontal grid size was 200 m for the along-fjord transect and 100 m for the across-fjord transect. A least-squares fit to a subtidal plus a semidiurnal harmonic, the lunar semidiurnal, was applied to the time series obtained at each grid point. This allowed separation of the tidal signal (amplitude and phase) from the nontidal signal for both the u (east) and v (north) components of the flow (e.g., Lwiza et al. 1991). Typical root-mean square errors between fit and observations were $< 0.01$ m $s^{-1}$ and the fit consistently explained $> 85\%$ of the variability of the flow. The subtidal flow derived from the fit was consistently similar, both quantitatively and qualitatively, to that obtained from straight means at each grid point. It made practically no difference to examine the fit-derived subtidal flow or the straight mean flow. Although bad weather hindered a sampling plan that would have allowed a reliable test of the hypothesis, the results still yielded some clue as to the causes of hypoxic waters reaching the upper water column.

## Data Description

The results of the data collection were separated by transect as they were sampled in different months and years. The bathymetric profile of the transect is described first in order to place the density and flow distributions in the context of bathymetric influences. The flow itself is presented in terms of tidal distributions as tidal ellipses and in terms of subtidal distributions.

## Along-fjord Transect

The depth at the southern end of the transect was $> 200$ m and the bottom sloped up gently toward the north until 1 km from the fjord's bend, where the bottom surged up to 100 m at the bend (Fig. 2). This shoaling had to do with the fact that in order to be straight, the trajectory could not remain in the middle of the channel at the bend, like at the southern and northern ends of the transect. North of the bend the bathymetry deepened rapidly to 155 m and then sloped gently to 180 m at the northern end of the transect. During the sampling period in March 2002, wind data from the closest meteorological station at Puerto Montt's airport, 50 km away, recorded wind speeds $< 5$ m $s^{-1}$ and directions that were primarily from the south and southwest. It could then be assumed that wind effects on the flow were unimportant during the sampling period.

During the sampling period a $<$ 4-m lens of low salinity water ($< 20$) was observed overlying the denser ocean water (Fig. 3). This lens was associated with large river discharge (700 $m^3$ $s^{-1}$) conditions and was separated from the underlying waters by a sharp pycnocline, of up to 6 kg $m^{-4}$, which varied in thickness with the tidal cycle but remained shallower than 10 m. The thermocline was broader than the halocline as temperature decreased from 14°C at the surface to 12.5°C at 10 m and then reached depth-independent values of 11°C at 20 m depth. Figure 3 shows that the time series at the southern end of the transect (station 1) had persistently higher salinity values than the northern location. These along-fjord differences were best illustrated by the surface salinity distributions in the time-distance domain as recorded by the underway CT that was attached to the catamaran (Fig. 4).

The surface waters showed a general salinity gradient from north to south, i.e., from head to mouth as expected in any fjord (Fig. 4). Surface temperature displayed the effects of diurnal heating as water cooled down toward the end of the experiment, which concluded soon after midnight (local time). These surface waters were nearly fresh with salinity values ranging between 0.5 and 5 along the transect. Such low salinities were likely the response to the relatively large Puelo River entering in the middle of the fjord. The lowest salinities shifted from the northernmost end of the transect at the beginning of the experiment to 2 km down the fjord during the second half of the sampling period; this second half was the period of largest horizontal salinity gradients at the surface, when relatively high salinity flood waters appeared in the study area. The coincidence of the lowest and highest salinity values was puzzling. The lowest salinity and temperature were likely associated with a mass of water released by the Puelo, but the mouth of the Puelo is to the south of the position where this mass was observed. More puzzling was the fact that the mass became evident at the onset of down-fjord surface flow, suggesting that its source was to the north of the Puelo mouth. This is worth

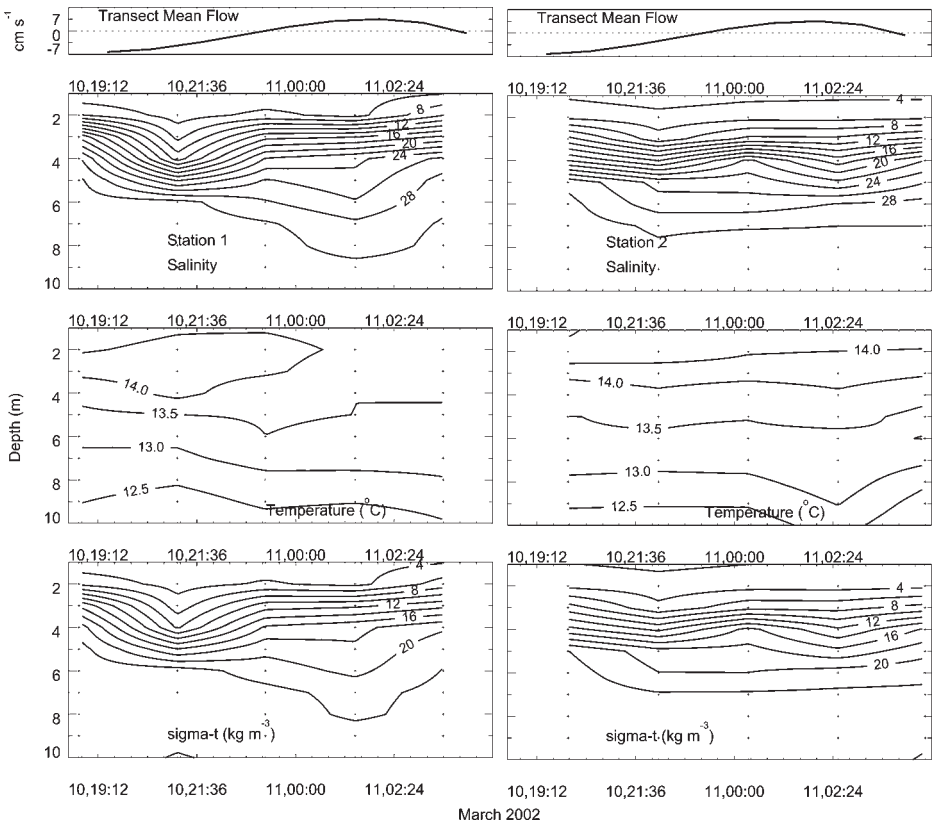


Fig. 3. Time series of transect-averaged flow (negative is ebb-directed) and of salinity, temperature, and density anomaly profiles at the extremes of the along-fjord transect. Station 1 is to the south of Station 2. Only the upper 10 m of the water column are shown for hydrography because properties change insignificantly below that depth.

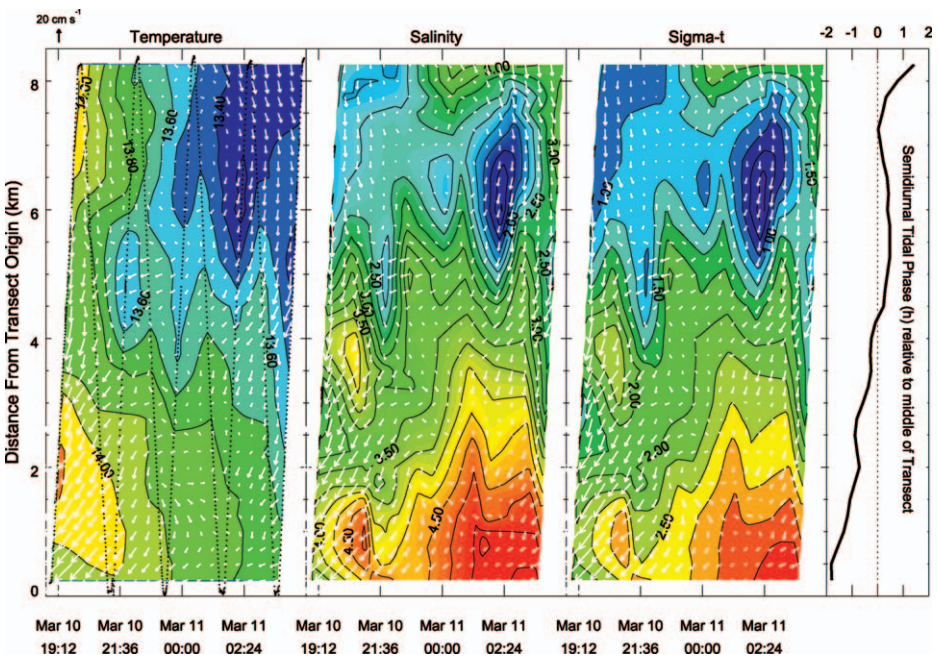


Fig. 4. Surface temperature, salinity, and density represented in the time-distance domain. Surface flow is represented together with each hydrographic variable. The semidiurnal tidal flow phase (in hours with respect to the middle of the transect) is represented at the right. The distance origin is at the southernmost end of the transect (station 1 in Fig. 3).

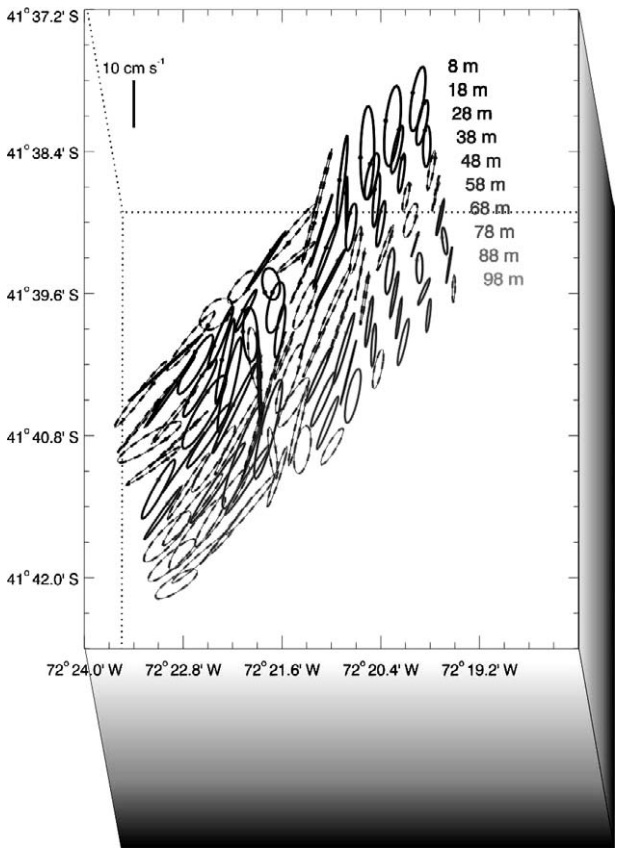


Fig. 5. Semidiurnal tidal ellipses for the along-fjord transect at different depths. Looking into the fjord. Ellipses are drawn every 650 m in the horizontal and from 8 to 98 m (every 10 m) in the vertical. The filled circle on each ellipse denotes the relative phase. Ellipses drawn with dashed lines rotate clockwise.

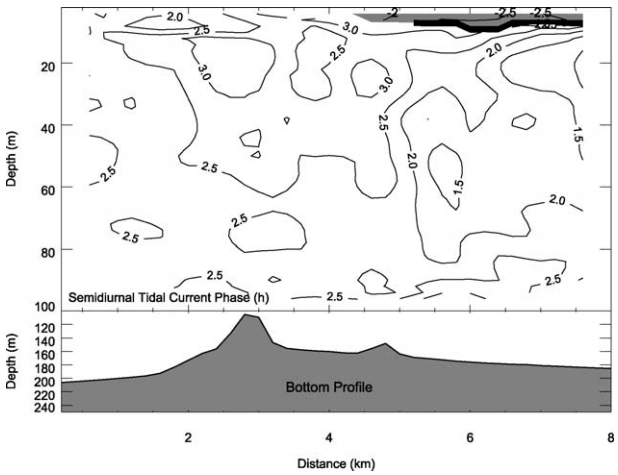


Fig. 6. Contours of phase (in hours) of semidiurnal tidal currents (derived from the ellipses) in the along-fjord transect. Contours are plotted at intervals of 0.5 h. The shaded area in the upper panel denotes a surface layer with negative phases. The bathymetry of the transect is shown for reference in the lower panel.

investigating in the future but could be related to the 2-h phase lag in semidiurnal tidal flow between both sides of the fjord bend. Such a phase lag was obtained by fitting a semidiurnal sinusoid to the observed flow at each point in the transect. The fit yielded $> 80\%$ variability explained by the semidiurnal oscillation throughout the transect.

The interactions between flood-tide waters and river-released waters associated with the lowest salinity and temperature caused horizontal density gradients of $5 \times 10^{-4}$ kg m$^{-4}$ at the surface (Fig. 4). The largest gradients of any given transect occupation throughout the observation period were observed in a front that persisted close to the middle of the transect, between 4 and 6 km. The front showed a puzzling oscillation of 2.5 h, derived from Fig. 4, that was unlikely produced by nonlinear tidal interactions because such interactions do not produce signals with those periods (Parker 1991). The possible cause of this oscillation is explored further in the discussion section.

The distribution of semidiurnal tidal currents throughout the transect was represented by semidiurnal tidal ellipses (Fig. 5). These were calculated as in Souza and Simpson (1996) from the least-squares harmonic analysis performed on the data. The amplitude of the semidiurnal tidal currents had a maximum of 10 cm s$^{-1}$ at the surface and a tendency to decrease northward and with depth. The orientation of these tidal currents was influenced by the coastline direction and the bathymetry. The greatest orientation change was observed at the bend, where the transect bathymetry shoals and where appreciable cross-channel tidal currents should develop according to the orientation of the tidal ellipses. The ellipticity of the currents was rather small everywhere, which indicated rectilinear tidal currents prevailing throughout the transect. The phases of the tidal ellipses showed appreciable changes from north of the bend to south of the bend, but were mainly restricted to a surface layer (Fig. 6). This surface layer coincided with the buoyant layer upstream of the bend, so the lag should be related to baroclinic effects on tidal currents.

The subtidal flow displayed a pattern consistent with estuarine circulation: net outflow at surface and net inflow underneath (Fig. 7). The surface outflow layer had a thickness of 40 m to the north of the bend and thinned markedly to $< 15$ m to the south of the bend. Typical outflow values were 5 cm s$^{-1}$ but increased to the south of the bend, as the outflow layer thinned. The inflow layer deepened as the water flowed around the bend. The

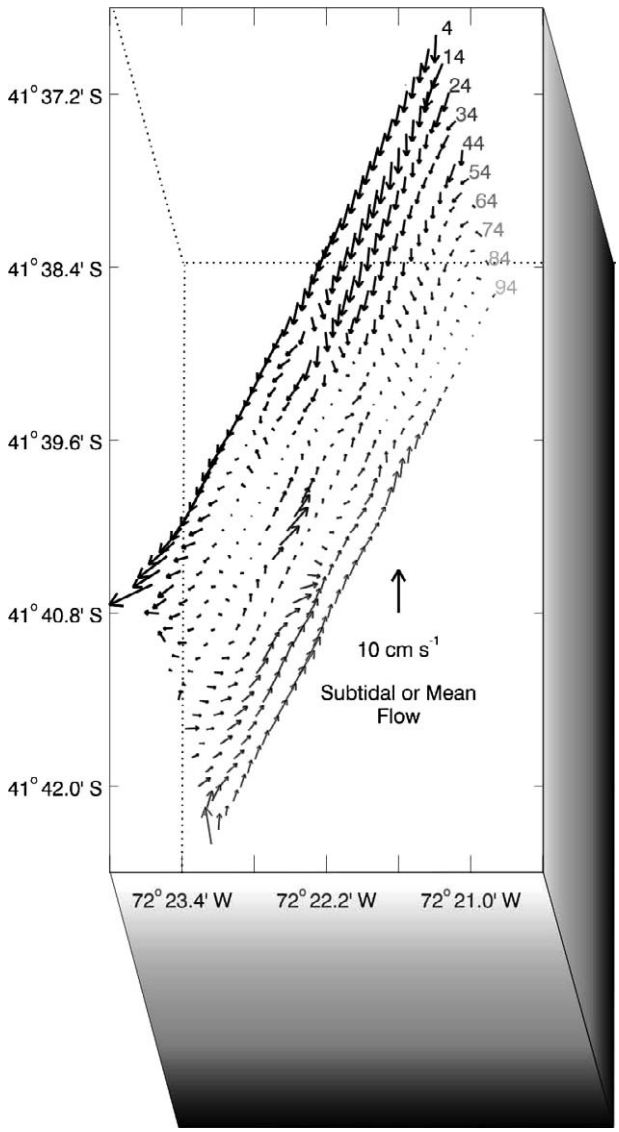


Fig. 7. Vector representation of subtidal flow in the along-fjord transect plotted at 10-m depth intervals (from 4 to 94 m). Looking into the fjord.

range of measurements was not able to track the core of net inflow as it moved northward of the bend, but still was able to document an increase with depth of net inflow. Also noteworthy was the change of orientation of net flows, following the geometry of the channel and in particular the localized cross-channel flows at the bend. This location is probably where the best across-fjord transfer of properties develops and where subpycnocline waters of low DO can get to the surface layer through pycnocline oscillations. This was explored further with the across-fjord transect measurements.

### Across-fjord Transect

The across-fjord transect was oriented roughly in the west-east direction. The depth at the western end of the transect, a few meters away from the coast, was 50 m and increased rapidly to a maximum depth of 175 m at 400 m from the transect origin (Fig. 2). Eastward of the deepest point, the bottom sloped up gently to the eastern coast of the fjord. During the sampling period in May 2004, wind data from Puerto Montt's airport showed weak winds ($< 5$ m s$^{-1}$) that played a negligible influence on the hydrographic distributions observed.

Hydrographic variables showed larger surface salinity values than in March 2002 (Fig. 8), because of the anomalously low river discharge (350 m$^3$ s$^{-1}$; León 2005). The lowest salinities ranged between 17 and 30 within a $<$ 4-m layer. As in March 2002, this stratified upper layer was separated from the underlying homogeneous waters by a sharp pycnocline of up to 4 kg m$^{-4}$. The pycnocline showed very small ($<$ 1 m) vertical excursions throughout the 12 h of measurements even though the lowest salinities appeared toward the end of the period. These low salinities strengthened the pycnocline but did not cause it to move downward. The temperature distributions showed maxima at 4 m deep as a consequence of autumn cooling at the surface. Still, temperature values in the upper 10 m across the fjord changed only from 11.2°C to 11.8°C throughout the sampling period. The lighter waters were observed at the eastern end of the transect (station 1 in Fig. 9) owing to its proximity to the Puelo River. The DO values obtained with the Idromar's probe showed larger oscillations than any of the other parameters measured. Low DO waters ($< 3$ ml l$^{-1}$) appeared near the surface on the western end of the transect (station 3) at the beginning of the sampling period and then on the eastern end (station 1) at the conclusion of sampling. This oscillation suggests that low DO can occur at both sides of the fjord. The possible cause for this oscillation is explored in the discussion section.

The semidiurnal tidal flows were also represented by tidal ellipses (Fig. 9). The distribution of the ellipses was relatively uniform in terms of amplitude and orientation of the semimajor axis. Typical tidal amplitudes were $<$ 10 cm s$^{-1}$ in the entire section, although they appeared to increase close to the coastline. The ellipse orientation changed a few degrees only near the western end of the section as currents followed the channel direction. Ellipses represented nearly rectilinear currents as their ellipticity was generally small. The phase of the semidiurnal tidal currents was relatively coherent and uniform throughout the section except near

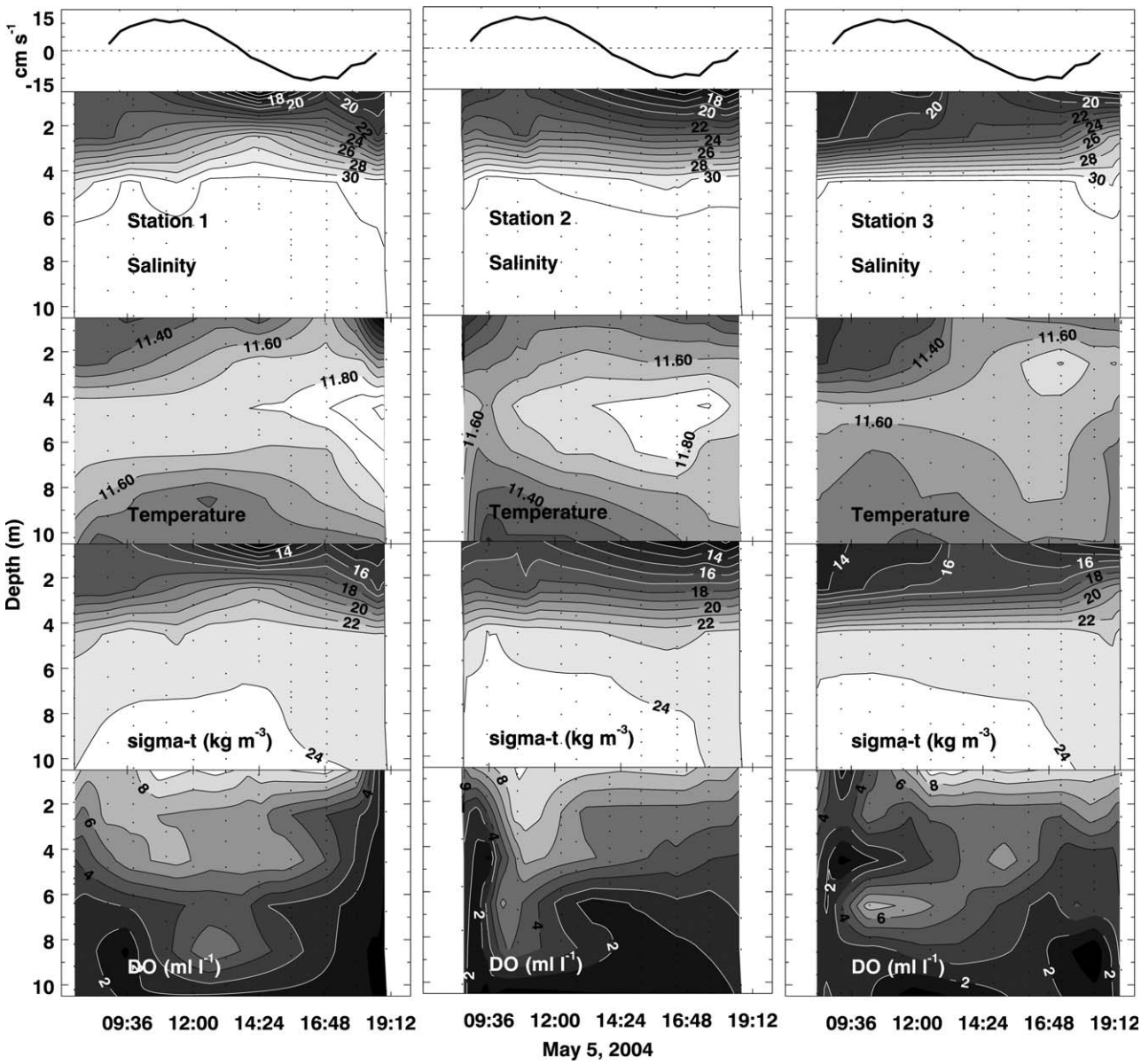


Fig. 8. Time series of sectionally averaged flow (negative is ebb-directed) and of salinity, temperature, density anomaly (sigma-t), and dissolved oxygen (DO) profiles at the extremes and in the middle of the across-fjord transect. Station 1 is to the east, station 2 is in the middle, and station 3 to the west. Only the upper 10 m of water column are shown for hydrography because properties change insignificantly below that depth.

the western end, at the bend, where the semidiurnal currents lead the rest of the section. This phase lead occurs because of the closest proximity of the bend to the tidal forcing boundary. The sense of rotation of the currents resembles the mean flow pattern. Roughly, the regions of net outflow displayed negative rotation and the regions of net inflow showed positive rotation. The reason for this remains unexplored.

The subtidal flows showed a picture that differed, in some ways, from the expected 2-layer estuarine circulation (Fig. 10). The subtidal flows displayed 3 layers: an easy-to-miss, thin ($< 8$ m) surface layer of net outflow, a middle layer 70 m thick of net inflow, and a bottom layer below 80 m depth of net outflow. The 3 layers were not apparent throughout the cross section. Near the western end of the transect, where the along-fjord transect cut through

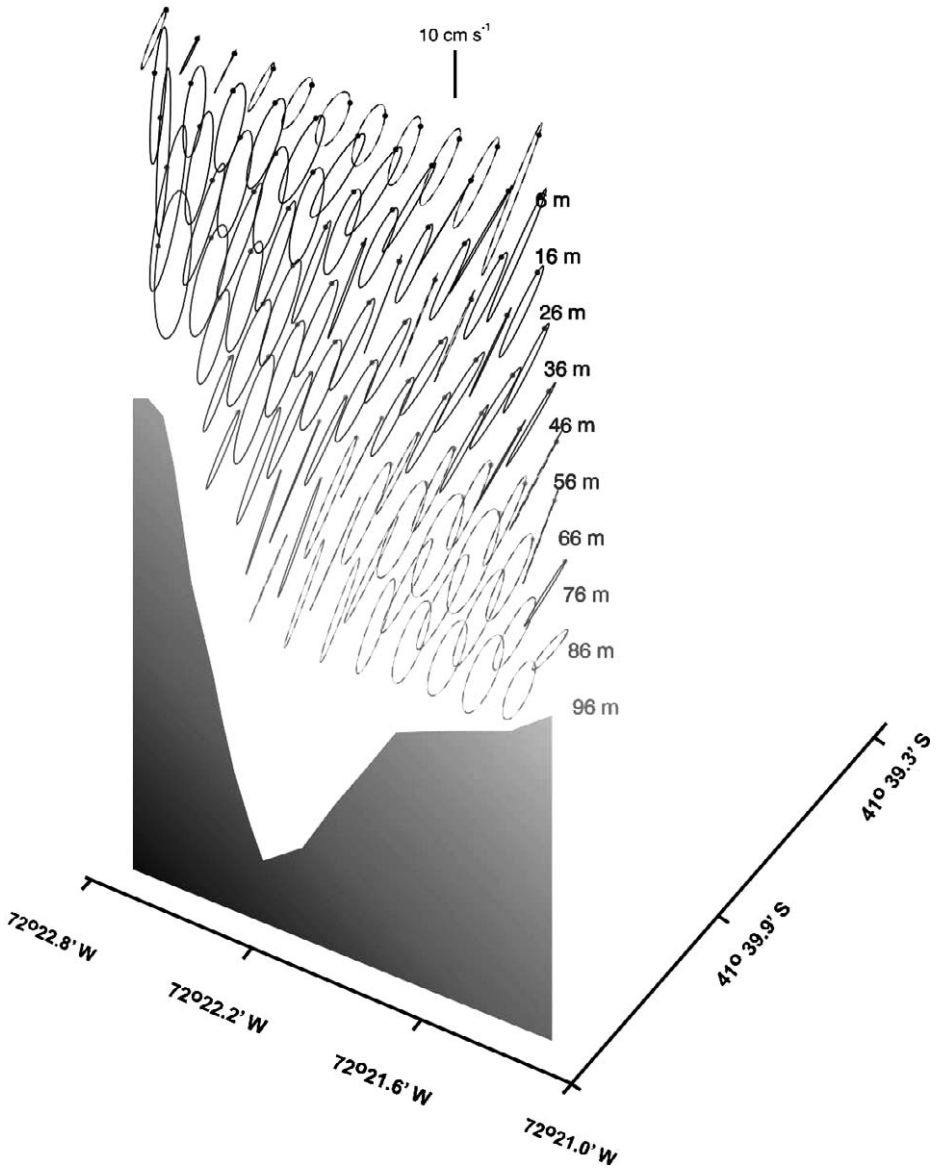


Fig. 9. Semidiurnal tidal ellipses for the across-fjord transect. Looking into the fjord. Ellipses are drawn every 200 m in the horizontal and from 6 to 96 m (every 10 m) in the vertical. The filled circle on each ellipse denotes the relative phase. Ellipses drawn with dashed lines rotate clockwise.

in March 2002 (0.6 km in Fig. 11), the subtidal flows exhibited 2 layers with net outflow throughout the upper 30 m and inflow underneath. The outflow between the depths of 10 and 30 m was apparently related to a clockwise recirculation that developed in the cross section at those depths. The 2-layer subtidal flow pattern over the western part of the section was consistent with that observed in March 2002 (Fig. 7), but overall, the 3-layer pattern was unexpected and is further explored in the discussion section.

Integrating the area of net inflow throughout the section yielded a volume inflow of 2000 $m^3 s^{-1}$, whereas the volume outflow measured was 1000 $m^3 s^{-1}$. There should have been a slight imbalance in favor of net volume outflow because of the river discharge (350 $m^3 s^{-1}$; León 2005). The current profiler recorded data down to depths of 100–110 m and missed a 50 m layer of what should have been net outflow, according to the pattern shown in Fig. 11. The measurements also missed the surface layer of most buoyant fluid that should

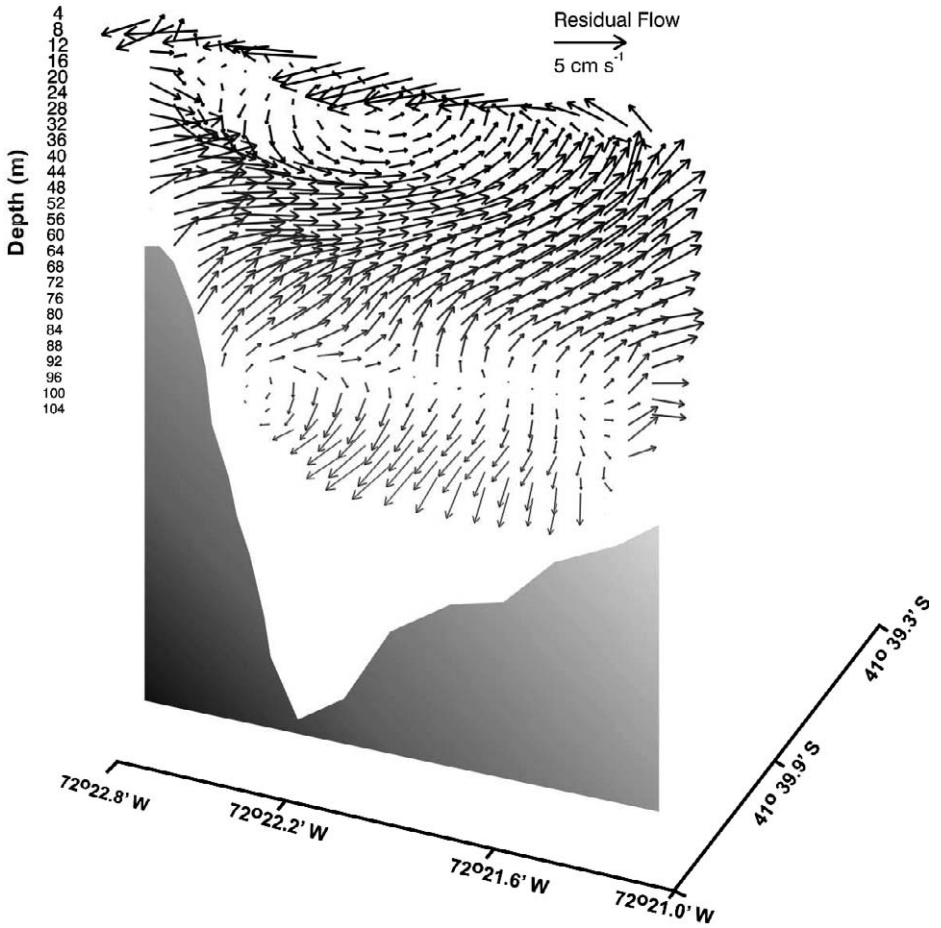


Fig. 10. Vector representation of subtidal flows in the across-fjord transect. Looking into the fjord. Horizontal spacing is 100 m and vertical spacing is 4 m (from 4 to 104 m).

have been associated with the strongest outflow. If such a buoyant layer is assumed to carry typical speeds of at least 10 cm $s^{-1}$ over a 3-m thick and 2-km wide layer, it would represent a volume outflow of at least 600 $m^3$ $s^{-1}$. Together, the lowermost and uppermost portions of the section that were unsampled should account for a volume imbalance in favor of net outflow.

The bend in the fjord coastline induced a coherent lateral flow throughout the transect (Fig. 11). The surface layer was directed toward the inside part of the channel, to the west (to the left on Fig. 11), and a lower layer was directed toward the outside part of the bend. Some indication of a third deep layer moving toward the west was also apparent. The lateral flow distribution suggested surface downwelling off the inside part of the bend and upwelling off the outside part of the bend. Underneath the surface layer, the lateral flow distribution was consistent with that expected from centrifugal accelerations experienced by tidal flows around capes or promontories (e.g., Signell and Geyer 1991; Seim and Gregg 1997; Lacy and Monismith 2001). Owing to centrifugal accelerations, surface flow should be directed away from the bend and subsurface flow should move into the bend. The overall distribution of observed lateral flow has two possible explanations. It is possible that the surface layer was driven by the discharge from the nearby Puelo River that moved across the fjord toward the inside part of the bend. Underneath that surface layer, the net inflow of oceanic waters could have been affected by centrifugal accelerations that caused lateral flow toward the outside part of the bend in the region of strongest inflow. As the along-fjord inflow decreased with depth, the lateral flow responded to the pressure gradient force toward the inside part of the bend. On the other hand, the effects from form drag could have caused the lateral flow distribution. Form drag could have been the reason for the surface outflow, and the inflow underneath, to follow the coastal morphology

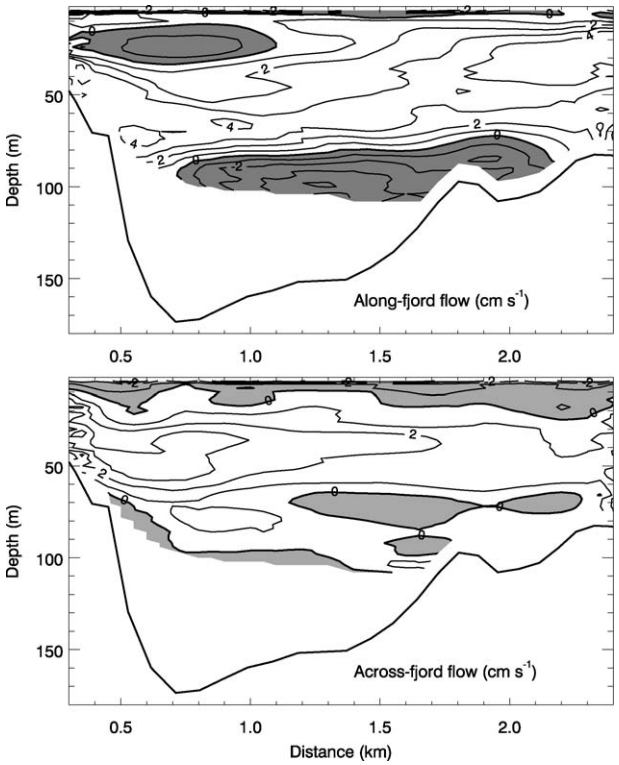


Fig. 11. Contours of the two horizontal components of the subtidal flow (in cm $s^{-1}$) in the across-fjord transect. Contour interval is 1 cm $s^{-1}$, looking into the fjord. Shaded areas in the along-fjord flow denote net outflows and in the across-fjord flow indicate motion to the left of the viewer.

instead of separating from it. This aspect and the other intriguing aspects suggested by the observations are addressed in the discussion.

## Discussion

Estuario Reloncaví can be regarded as a homogeneous system, for the most part, with a thin layer ($<$ 5 m thick) of buoyant water slipping seaward. The persistence of a relatively thin, buoyant layer is allowed by relatively weak tidal currents (10 cm $s^{-1}$) despite the relatively large tidal amplitudes (up to 3.5 m) in the area. Tidal currents are weak because of the deep nature of the fjord and are not energetic enough to mix the buoyant waters. On the basis of continuity, tidal current amplitudes $u_0$ are proportional to the surface area of the fjord $Y$, to the frequency of tidal forcing $\sigma$, and to the tidal amplitude $a$, and inversely proportional to the cross-sectional area $A$ (Stigebrandt 1977). In other words, $u_0 = aY\sigma/A$, and using a value for $a$ of 1.8 m for the semidiurnal tidal amplitude, a $Y$ value of $1.1 \times 10^8$ $m^2$, $\sigma$ value of $1.4 \times 10^{-4}$ $s^{-1}$ for the semidiurnal forcing, and $A$ value of $3.4 \times 10^5$ $m^2$ yields semidiurnal tidal currents of 0.08 m $s^{-1}$, or close to those observed. Wind stress or river pulses may force deepening of the buoyant layer by several meters but the layer should recover its slenderness soon after the river pulse or the wind relaxes.

In this study, the first in Reloncaví fjord involving current velocity measurements, there were four aspects of the measurements that were revealing: the 2.5-h oscillation of the surface front observed in the along-fjord transect (Fig. 4); the large semidiurnal phase change at the bend (Figs. 4 and 6); the intriguing 3-layer subtidal exchange (Figs. 10 and 11); and the pattern of across-fjord flows (Fig. 11). The oscillation of the surface front may be attributed to the natural period of oscillation for internal motion across the fjord. This period is given by $2W/C_i$, where $W$ is the width of the fjord (2.3 km at the observation section) and $C_i$ is the speed of the first mode internal wave (0.52 m $s^{-1}$). In turn, $C_i$ is obtained from $[g' h_o]^{1/2}$, where $h_o$ is the depth of the buoyant layer (4 m) and $g'$ is the reduced gravity, which equals $g\Delta\rho/\rho$, where $g$ is the acceleration due to gravity (9.8 m $s^{-2}$), $\Delta\rho$ is the density contrast between upper and lower layers (7 kg $m^{-3}$), and $\rho$ is a reference density (1020 kg $m^{-3}$). The period obtained with the values given above is 2.5 h, remarkably the same as the one observed in Fig. 4. Inclusion of a 2.5 h cycle to the fit for surface flows in Fig. 4 improves the goodness of fit in the area between 3 and 6 km from 80% to $>$ 90%. Because the tidal currents are so weak, this lateral oscillation may have been triggered by a pulse of the Puelo River because the oscillation was not apparent in the CTD data of May 2004 (Fig. 8), when buoyancy forcing was substantially weaker. It also could potentially be triggered by wind forcing. The oscillation was most apparent in a portion of the March 2002 transect where no CTD casts, only underway surface measurements, were made (Fig. 4). Detailed inspection of the hydrographic time series measured at the ends of the transect suggested a weak oscillation. As with all of the four intriguing aspects of the results, this aspect requires further study. Although the oscillations were not well resolved in this study, this finding will hopefully be the target of future studies.

The large semidiurnal phase of the tidal currents only appeared at the surface layer (Figs. 4 and 6). In most of the section, below that surface layer, the phases were relatively uniform (Fig. 6). Such phase lag developed, i.e., the phase changed most rapidly, in the region of the front that oscillated with a 2.5 h period. The front itself should produce currents on the order of the tidal currents. The front-induced currents should distort and most likely overwhelm the semidiurnal tidal currents. These currents should then change dramatically from one side of the front to the other. Such a change of currents across the front would ultimately result in the phase change observed.

The 3-layer pattern of net along-fjord flows displayed in Figs. 10 and 11 is perhaps the most revealing result of this study. The pattern was consistent with that observed in Seno Aysen, another fjord of the Chilean Inland Sea (Cáceres et al. 2002) and in Jøsenfjord, Norway (Svendsen and Thompson 1978). In Seno Aysen, the 3-layer pattern favored a larger volume of net outflow and was attributed to up-fjord wind forcing that drove bottom layer outflow through a sea level setup. In Jøsenfjord, the 3-layer pattern was also attributed to wind forcing. In Reloncaví, winds were weak during the study period so the pattern could not be attributed to this type of forcing. Besides, the 3-layer pattern also has been observed in several other channels of the Chilean Inland Sea (Cáceres personal communication) under weak wind conditions. This pattern could be attributed instead to tidal residuals that tend to oppose the typical estuarine circulation (e.g., Ianniello 1977, 1978). Following Ianniello (1977), Reloncaví fjord can be considered a weakly nonlinear system as determined by the ratio of tidal amplitude $a$ to depth $H$, which is 0.04. More importantly, it can also be considered a frictional system as determined by the ratio of $H$ to the frictional length scale $F$. This ratio, which is Ianniello's parameter $d_0$ and considered to be fundamental to determine frictional effects on tidal and subtidal flows, equals $H[2N_{zm}/\sigma]^{-1/2}$, where $N_{zm}$ is a vertical eddy viscosity approximated by the relation

$$N_{zm} = 8C_dHu_0/(3\pi).$$

In this expression, $C_d$ is the nondimensional bottom drag coefficient (0.0025), and $u_0$ is the tidal current amplitude (0.1 m s$^{-1}$). For depths $H$ of 100 to 200 m in Estuario Reloncaví, $d_0$ may range between 5 and 8. In a channel where the tide reflects at a wall, this range of $d_0$ yields tidal residuals of 2 layers ($d_0$ of 5) and 3 layers ($d_0$ of 6, 7, and 8; Fig. 10 of Ianniello 1977) consistent with the pattern observed here. For the 2-layer tidal residual pattern, inflow appears in a surface layer and outflow underneath. This pattern would oppose the thin, buoyant layer outflow but coincide with the regions of observed net inflow below the buoyant layer and outflow observed toward the bottom. The 3-layer tidal residual pattern consists of outflow at surface and near the bottom, and net inflow in a layer between surface and bottom, as observed in Estuario Reloncaví. It is proposed here that the lower layer outflow observed in Reloncaví and in other channels of the Inland Sea is produced by tidal nonlinearities caused by tidal reflection at the head. This shall be the focus of a future study.

The pattern of across-fjord flows may be the result of centrifugal accelerations underneath the surface buoyant layer (e.g., Seim et al. 2002; Lacy et al. 2003) or of streamwise bathymetric changes that cause form drag (e.g., Edwards et al. 2004). With sharp coastline changes and relatively uniform bathymetry, the centrifugal accelerations $U^2/Rc$, where $U$ is a typical tidal current amplitude and $Rc$ is the radius of coastline curvature, should dominate the dynamics. For tidal currents observed, a typical value of centrifugal accelerations was $0.6 \times 10^{-5}$ m s$^{-2}$ with a generous $U$ of 0.2 m s$^{-1}$ and $Rc$ of 7 km from coastline geometry at Reloncaví's bend. This estimate is smaller than the Coriolis accelerations $fU$ of $1.9 \times 10^{-5}$ m s$^{-2}$ with an $f$, the Coriolis parameter, of $9.5 \times 10^{-5}$ s$^{-1}$ for a latitude of 41°. In the case that form drag is important, the mean flow would follow the bathymetry and coastline orientations. Form drag accelerations are given by $C_fU^2/H$, where $C_f$ is a drag coefficient. For drag accelerations to be important the ratio $C_fRc/H$, which is the ratio of drag to centrifugal accelerations, has to be $\geq 1$. Using $Rc$ of 7 km and $H$ of 100 m, it follows that $C_f$ needs to be $\geq 1.4 \times 10^{-2}$ for drag to be relevant and for the currents to follow the coastline orientation, as observed in the along-fjord transect (Figs. 4 and 7). This was within the range of values proposed by Edwards et al. (2004) for Three Tree Point in Puget Sound, which has similar bathymetric characteristics to Reloncaví's bend. Because the value of $C_f$ has to be large compared to the canonical bottom drag coefficient of $2.5 \times 10^{-3}$, then form drag and not bottom drag would cause the across-fjord flow pattern observed. This would have to be explored with detailed hydrographic observations around the bend similar to those of Edwards et al. (2004).

In addition to the four revealing aspects of the measurements, there is a need to propose residence time estimates to, in turn, be able to determine the carrying capacity of the system, which is heavily used by the salmon culture industry. Residence times have been calculated on the basis of mass conservation for the lower layer and in terms of a buoyant particle traveling the extent of the fjord for the upper layer. On the basis of mass conservation, the net volume inflow to the fjord $V_{in}$ is a function of the river discharge $R$, the outflowing salinity $S_{out}$, and the inflowing salinity $S_{in}$:

$$V_{in} = RS_{out}/(S_{in} - S_{out}).$$

Using $R$ of 900 m$^3$ s$^{-1}$, $S_{out}$ of between 3 and 20, and $S_{in}$ of 30, yields a $V_{in}$ of 100 to 1800 m$^3$ s$^{-1}$. The residence time is given by the volume $E$ of the fjord ($1.7 \times 10^{10}$ m$^3$) divided by $V_{in}$, which yields between 5.3 yr and 109 d. If the value of $V_{in}$ of 2000 m$^3$ s$^{-1}$ measured in the across-fjord transect is used,

instead of using mass conservation, then the residence time is 98 d. This estimate is similar to the mass conservation value obtained with the high $S_{out}$. The observed pattern of net inflows and outflows is expected to be influenced by nonlinear tidal effects, not only by density-driven currents, so the 100-d estimate may be more representative of actual conditions. In terms of a buoyant particle traveling the 55 km of the fjord at 5 cm $s^{-1}$, it would take between 12 and 13 d for that particle to go from head to mouth of the fjord. These estimates do not include the effect of wind, which may be important especially in the upper layer.

## Conclusions

The first study that has investigated flow patterns in the Reloncaví fjord, the most equatorward Chilean fjord, revealed intriguing phenomena at intratidal and subtidal time scales. At intratidal scales, observations suggested a 2.5-h oscillation of a surface front (Fig. 4) that may be associated with lateral seiching triggered by winds or by discharge from the Puelo River. Also intratidally, the semidiurnal currents near the surface exhibited a 2 h phase change (Figs. 4 and 6) related to the general position of the front, just upstream of the coastline bend. At subtidal scales, a 3-layer pattern of water exchange consisted of net outflow through a thin surface layer and also through a deep layer, with net inflow between the two outflow layers (Fig. 11). This pattern, which was consistent with observations at other channels and fjords of the Chilean Inland Sea, was attributed to nonlinear tidal effects arising from tidal wave reflection at the head of the fjord. Also at subtidal scales, the across-fjord flow pattern at the coastline bend (Fig. 11) could have been attributed to form drag effects (more likely) or centrifugal accelerations. All these conclusions are suggestive, as they are related to a very limited sample of the possible variability in the system.

## Acknowledgments

This study was funded by the Instituto Tecnológico del Salmon (INTESAL) in Chile and by the Núcleo Milenio FORECOS in Chile. A. Valle-Levinson was supported by National Science Foundation grant 9983685. The support of the Ocean, Earth and Atmospheric Sciences at Old Dominion University for the participation of N. Sarkar is thankfully acknowledged. J. L. Blanco, D. Salas, H. Perales, I. Arismendi, C. Leal, M. Castillo, and V. Barrera greatly contributed in the data collection. M. Cáceres of the Chilean Naval Hydrographic Service kindly provided the bathymetry. The comments of two anonymous reviewers helped to improve the contents and presentation of this work.

## Literature Cited

Bathurst, J. C., C. R. Thorne, and R. D. Hey. 1977. Direct measurements of secondary currents in river bends. *Nature* 269: 504–506.

Cáceres, M., A. Valle-Levinson, and L. Atkinson. 2003. Observations of cross-channel structure of flow in an energetic tidal channel. *Journal of Geophysical Research* 108:3114, doi:10.1029/2001JC000968.

Cáceres, M., A. Valle-Levinson, H. H. Sepulveda, and K. Holderied. 2002. Transverse variability of flow and density in a Chilean fjord. *Continental Shelf Research* 22:1683–1698.

Chant, R. J. and R. E. Wilson. 1997. Secondary circulation in a highly stratified estuary. *Journal of Geophysical Research* 102: 23207–23215.

Edwards, K. A., P. MacCready, J. N. Moum, G. Pawlak, J. M. Klymak, and A. Perlin. 2004. Form drag and mixing due to tidal flow past a sharp point. *Journal of Physical Oceanography* 34:1297–1312.

Geyer, W. R. 1993. Three-dimensional tidal flow around headlands. *Journal of Geophysical Research* 98:955–966.

Geyer, W. R. and R. Signell. 1990. Measurements of tidal flow around a headland with a shipboard acoustic Doppler current profiler. *Journal of Geophysical Research* 95:3189–3197.

Ianniello, J. P. 1977. Tidally induced residual current in estuaries of constant breadth and depth. *Journal of Marine Research* 35: 755–786.

Ianniello, J. P. 1978. Tidally induced residual current in estuaries of variable breadth and depth. *Journal of Physical Oceanography* 9: 962–974.

Joyce, T. M. 1989. On in situ calibration of shipboard ADCPs. *Journal of Atmospheric Oceanic Technology* 6:169–172.

Lacy, J. and S. Monismith. 2001. Secondary currents in a curved, stratified estuarine channel. *Journal of Geophysical Research* 106: 31283–31302.

Lacy, J., M. Stacey, J. R. Burau, and S. Monismith. 2003. Interaction of lateral baroclinic forcing and turbulence in an estuary. *Journal of Geophysical Research* 108: doi:10.1029/2002JC001392.

León, J. E. 2005. Influencia del caudal del Río Puelo sobre la salinidad y la concentración de oxígeno disuelto en el Estuario de Reloncaví, Llanquihue, Chile, M.S. Thesis. Universidad Austral de Chile, Valdivia, Chile.

Lwiza, K. M. M., D. G. Bowers, and J. H. Simpson. 1991. Residual and tidal flow at a tidal mixing front in the North Sea. *Continental Shelf Research* 11:1379–1395.

Malone, T. C., W. M. Kemp, H. W. Ducklow, W. R. Boynton, J. H. Tuttle, and R. B. Jonas. 1986. Lateral variation in the production and fate of phytoplankton in a partially stratified estuary. *Marine Ecology Progress Series* 32:149–160.

Milliman, J. D., C. Rutkowski, and M. Meybeck. 1995. River discharge to the sea. A global river index (GLORI). LOICZ Reports and Studies, Texel, The Netherlands.

Niemeyer, H. and P. Cereceda. 1984. Hidrografía, p. 1–313. *In* I. G. Militar (ed.), Geografía de Chile, Volume VIII. Instituto Geografía de Chile, Santiago, Chile.

Parker, B. B. 1991. The relative importance of the various nonlinear mechanisms in a wide range of tidal interactions (review), p. 237–268. *In* B. Parker (ed.), Tidal Hydrodynamics. John Wiley and Sons, New York.

Seim, H., J. O. Blanton, and T. Gross. 2002. Direct stress measurements in a shallow, sinuous estuary. *Continental Shelf Research* 22:1565–1578.

Seim, H. and M. Gregg. 1997. The importance of aspiration and channel curvature in producing strong vertical mixing over a sill. *Journal of Geophysical Research* 102:3451–3472.

Signell, R. and W. R. Geyer. 1991. Transient eddy formation around headlands. *Journal of Geophysical Research* 96:2561–2575.

Soto, D. and F. Norambuena. 2004. Evaluation of salmon farming effects on marine systems in the inner seas of southern Chile: A large-scale mensurative experiment. *Journal of Applied Ichthyology* 20:493–501.

SOUZA, A. J. AND J. H. SIMPSON. 1996. The modification of tidal ellipses by the stratification in the Rhine ROFI. *Continental Shelf Research* 16:997–1007.

STIGEBRANDT, A. 1977. On the effect of barotropic current fluctuations on the two-layer transport capacity of a constriction. *Journal of Physical Oceanography* 7:118–122.

SVENDSEN, H. AND R. O. R. Y. THOMPSON. 1978. Wind-driven circulation in a fjord. *Journal of Physical Oceanography* 8:705–712.

THORNE, C. R. AND R. D. HEY. 1979. Direct measurements of secondary currents at a river inflexion point. *Nature* 280:226–228.

VALLE-LEVINSON, A. AND L. ATKINSON. 1999. Spatial gradients in the flow over an estuarine channel. *Estuaries* 22:179–193.

VALLE-LEVINSON, A. AND J. L. BLANCO. 2004. Observations of wind influence on exchange flows in a strait of the Chilean Inland Sea. *Journal of Marine Research* 62:721–741.

## SOURCE OF UNPUBLISHED MATERIALS

CÁCERES, M. personal communication. Chilean Naval Hydrographic Service Errazuriz 232, Casilla 324, Valparaiso, Chile.

*Received, July 29, 2005*
*Revised, January 9, 2006*
*Accepted, November 20, 2006*